Journal of Organometallic Chemistry 895 (2019) 55–63

Contents lists available at ScienceDirect

Journal of Organometallic Chemistry

journal homepage: www.elsevier.com/locate/jorganchem

$Fe_{3-x}Ti_xO_4$-supported sulfamic acid nanoparticles: New magnetic nanocatalyst for the synthesis of hexahydroquinolines

Davood Azarifar [a], Younes Abbasi [a, *], Mehdi Jaymand [b, **], Mohammad Ali Zolfigol [a], Masoumeh Ghaemi [a], Omolbanin Badalkhani [a]

[a] Faculty of Chemistry, Bu-Ali Sina University, Hamedan, Iran
[b] Nano Drug Delivery Research Center, Health Technology Institute, Kermanshah University of Medical Sciences, Kermanshah, Iran

ARTICLE INFO

Article history:
Received 2 February 2019
Received in revised form
14 May 2019
Accepted 21 May 2019
Available online 22 May 2019

Keywords:
Titanomagnetite
Nanocatalyst
Hexahydroquinolines
Sulfamic acid
Reusability

ABSTRACT

A novel acidic nanocatalytic system, sulfamic acid-functionalized $Fe_{3-x}Ti_xO_4$ magnetic nanoparticles (MNPs), were synthesized through one-pot reaction of $Fe_{3-x}Ti_xO_4$ MNPs with 3-chloropropyltrimethoxysilane and imidazolidine-2,4-dione followed by functionalization with chlorosulfonic acid. The structure of this newly synthesized nanocatalyst was established by several analysis methods including, Fourier-transform infrared (FTIR) and energy-dispersive X-ray (EDX) spectroscopies, transmission (TEM) and scanning (SEM) electron microscopies, thermal gravimetric (TG), X-ray diffraction (XRD), and vibrating sample magnetometer (VSM). The potential catalytic ability of this nanocatalyst was evaluated in one-pot four-component condensation reaction between aromatic aldehydes, dimedone, alkyl acetoacetates and ammonium acetate in order to synthesis of hexahydroquinoline derivatives. The reactions proceeded smoothly under solvent-free condition offering excellent yields of corresponding hexahydroquinolines successfully. In addition, the fabricated nanocatalyst exhibited excellent reusability up to four subsequent runs.

1. Introduction

Over the last few decades, development of environmentally benign and eco-friendly processes and catalysts has emerged as increasingly important goal in the chemistry domain [1,2]. Recently, an area of intense catalytic endeavor in organic synthesis has emphasized the use and design of the catalysts immobilized on various nano-sized supports possessing high performance of catalytic activity and stability compared to unsupported counterparts [3]. Among the solid nanomaterials used as supports for a wide variety of catalysts, magnetic nanoparticles (MNPs) have attracted great deal of interest as efficient catalysts and supports throughout the scientific as well as industrial communities due to their unique size, high surface-to-volume ratio, good biocompatibility, low toxicity, efficient recyclability, and coordinated parts which provide a larger number of active sites per unit area in comparison with their corresponding bulk materials [4–18]. Moreover, MNPs can be easily separated from the reaction mixture simply using an external magnet bar. This strategy avoids the tedious process of isolation via filtration or centrifugation for such small NPs [19,20]. However, the main problem regarding the application of MNPs is their quick aggregation into large bunches that leads to lose their unique properties. To circumvent this problem and preserve their nanoscale properties, their surface is usually shielded with organic (*e.g.,* silan coupling agent) or inorganic materials (*e.g.,* silica) to form core-shell structures [21,22].

Among the most extensively studied MNPs as the core magnetic support to immobilize various catalysts, Fe_3O_4 [23–27] and Fe_2O_3 [28–30] NPs have received enormous attention because of their simple synthesis, low cost, and relatively large magnetic susceptibility [31–35]. In addition, the incorporation of Ti^{4+} cations into the Fe_3O_4 MNPs structure in order to produce $Fe_{3-x}Ti_xO_4$ MNPs significantly increase the relative number of surface hydroxyl groups that lead to improve physicochemical features of the final nanomaterial [23,26].

A wide variety of pharmacologically active heterocyclic compounds embrace a quinoline scaffold in their framework [36,37]. Many of these compounds possesses antibacterial, antihypersensitive, anti-malarial, anti-inflammatory and anti-asthmatic activities [38,39], and tyrosine kinase PDGF-RTK inhibiting

* Corresponding author.
** Corresponding author.
E-mail addresses: younes.abbasi@yahoo.com (Y. Abbasi), m_jaymand@yahoo.com, m.jaymand@gmail.com (M. Jaymand).

https://doi.org/10.1016/j.jorganchem.2019.05.020
0022-328X/

properties continue to spur synthetic efforts regarding their acquisition [40,41]. In addition, quinolones are useful synthons for the preparation of various industrial products such as nanostructures and polymers with enhanced electronic, optical and mechanical properties [42]. Therefore, these important industrial, pharmacological and synthetic values have rendered the quinolones attractive as synthetically challenging research targets. Various synthetic strategies including, Skraup, Doebner von Miller, Combs, and Friedländer procedures [43–45], as well as one-pot multi-component reactions (MCRs) have been introduced for the synthesis of quinolones. Among these, MCRs catalyzed by various catalysts such as silica-bonded imidazolium-sulfonic acid chloride [46], hafnium (IV) bis(perfluorooctanesulfonyl)imide complex [47], scandium triflate [48], protic pyridinium ionic liquid [49], magnetite–ceria nanocatalyst [50], nanometasilica disulfuric acid and nanometasilica monosulfuric acid sodium salt [51], and ZrO_2 nanoparticles [52] are particular of interest.

In continuation of our ongoing studies towards the development of efficient and environmentally friendly synthesis of heterogeneous naocatalysts and their application in organic transformations and heterocyclic compounds synthesis [53–58], herein, we report the synthesis and characterization of imidazolidine-2,5-dione-1-sulfamic acid-functionalized $Fe_{3-x}Ti_xO_4$ MNPs (denoted as $Fe_{3-x}Ti_xO_4$-SO_3H MNPs) and their application as efficient nanocatalyst for the synthesis of hexahydroquinolines **5a-m** through a one-pot four-component reaction between aromatic aldehydes, dimedone, alkyl acetoacetates and ammonium acetate (Scheme 1).

2. Results and discussion

2.1. Catalyst characterization

In the present work, we have synthesized $Fe_{3-x}Ti_xO_4$-SO_3H as magnetic heterogeneous nanocatalyst. As illustrated in Scheme 2, we initially synthesized $Fe_{3-x}Ti_xO_4$ MNPs by the reaction of an equimolar amounts of $FeSO_4 \cdot 7H_2O$ and $TiCl_4$ in acidic solution with hydrazine monohydrate [53]. In the next stage, the surface of $Fe_{3-x}Ti_xO_4$ MNPs were modified using 3-silylpropylhydantoin (SPH) *via* one-pot reaction with 3-chloropropyltrimethoxysilane and imidazolidine-2,4-dione (hydantoin). Finally, the resulted NPs were sulfonated by treatment with chlorosulfonic acid. It is interesting to know that, the presence of Ti^{+4} cations in the structure of NPs can increase the number of superficial hydroxyl groups [59], and improve the loading capacity of sulfonic acid groups on the surface of the titanomagnetite NPs (4.1–5.5 $mmolg^{-1}$) compared with the magnetite Fe_3O_4 NPs (1.76 $mmolg^{-1}$) [60], and magnetite silica-coated Fe_3O_4 NPs (0.32 $mmolg^{-1}$) [61].

The structure of the synthesized nanocatalyst was fully characterized by different analysis methods including, FTIR spectroscopy, EDX, SEM, TEM, XRD, VSM, and TGA as follows. The FTIR spectra of the $Fe_{3-x}Ti_xO_4$ NPs (a), SPH-functionalized $Fe_{3-x}Ti_xO_4$ (b), and $Fe_{3-x}Ti_xO_4$-SO_3H MNPs (c) are shown in Fig. 1. Comparison between three spectra clearly confirms the successful conjugation of 3-(3-silyl propyl) hydantoin-1-sulfonic acid onto the surface of the $Fe_{3-x}Ti_xO_4$ NPs. The peaks shown at 3418, 587 and 796 cm^{-1} in the FTIR spectrum of the $Fe_{3-x}Ti_xO_4$ NPs are assigned to the O–H, Fe–O and Ti–O stretching vibrations, respectively (Fig. 1**a**). The SPH-functionalized $Fe_{3-x}Ti_xO_4$ and $Fe_{3-x}Ti_xO_4$-SO_3H exhibited the same stretching vibrations at 3415 (O–H), 684 (Fe–O), and 764 (Ti–O) cm^{-1} (Figs. 1**b**) and 3422 (O–H), 594 (Fe–O), 764 (Ti–O) cm^{-1} (Fig. 1**c**), respectively. The appearance of aliphatic C–H stretching vibrations at 2934 to 3058 cm^{-1} rejoin along with the $-CH_2$ bending vibrations at 1457 and 1460 cm^{-1} in FTIR spectra provides evidence for the successful attachment of silylpropyl linker to the surface of the $Fe_{3-x}Ti_xO_4$ NPs.

The successful attachment of the hydantoin moiety onto the surface of these NPs is justified by the appearance of the absorption bands at 1704 and 1766 cm^{-1} for the SPH-functionalized $Fe_{3-x}Ti_xO_4$ and at 1702 and 1743 cm^{-1} for the $Fe_{3-x}Ti_xO_4$-SO_3H MNPs, respectively that related to the C=O stretching vibrations. In addition, the appearance of two absorption bands at 988 and 1210 cm^{-1} in the FTIR spectrum of $Fe_{3-x}Ti_xO_4$-SO_3H MNPs (Fig. 1**c**) confirm the presence of the sulfamic acid groups in the sample.

The elemental composition of the synthesized $Fe_{3-x}Ti_xO_4$-SO_3H nanocatalyst was investigated using EDX analysis as shown in Fig. 2. The EDX analysis clearly indicates the peaks for Si, Ti, Fe, C, N, S, and O elements that verify the successful formation of $Fe_{3-x}Ti_xO_4$-SO_3H MNPs. The results obtained from EDX analysis is summarized in Table 1.

The morphological structure as well as size distribution of the synthesized $Fe_{3-x}Ti_xO_4$-SO_3H nanocatalyst were investigated using SEM as well as TEM analysis as illustrated in Fig. 3. The SEM image exhibited that the catalyst was made up of spherical and nanometer-sized particles in the range of 35 ± 10 nm. In contrast, the TEM image exhibited spherical core-shell morphology for these NPs. The average diameters of core and shell are about 60 ± 10 and 70 ± 10 nm, respectively. This morphology as well as diameter can provided high surface area for the immobilization of organic compounds onto the NPs for efficient catalysis of various reactions.

It is well established that the catalytic activity can be strongly affected by crystallinity of the catalyst. The crystallinity of the synthesized $Fe_{3-x}Ti_xO_4$-SO_3H nanocatalyst was studied using XRD analysis as illustrated in Fig. 4. The successful synthesis of crystalline $Fe_{3-x}Ti_xO_4$-SO_3H nanocatalyst was approved through the appearance of some diffraction peaks at $2\theta = 30.4$, 35.8, 43.5, 53.8, 57.5, and 63.1°. It should be pointed out that the organic shell around the $Fe_{3-x}Ti_xO_4$-SO_3H MNPs act as impurity that reduced the crystallinity of the nanocatalyst. Despite, the fabricated nanocatalyst has excellent crystallinity according to XRD pattern.

The magnetic properties of the $Fe_{3-x}Ti_xO_4$ MNPs and $Fe_{3-x}Ti_xO_4$-SO_3H MNPs were measured using VSM equipment at 300 K in the applied field sweeping range of −10000 to 10000 Oe. The saturation magnetization (δ_s) of the $Fe_{3-x}Ti_xO_4$ MNPs and $Fe_{3-x}Ti_xO_4$-SO_3H MNPs were obtained to be 33.85 and 14.02 $emu.g^{-1}$, respectively. This reduction in the δ_s value is originated from the effective loading of precursors on the surface of $Fe_{3-x}Ti_xO_4$ MNPs that verify the successful synthesis of $Fe_{3-x}Ti_xO_4$-SO_3H MNPs. In spite of this reduction, the catalyst still retains sufficient magnetism to be efficiently separated from the solution simply using an external

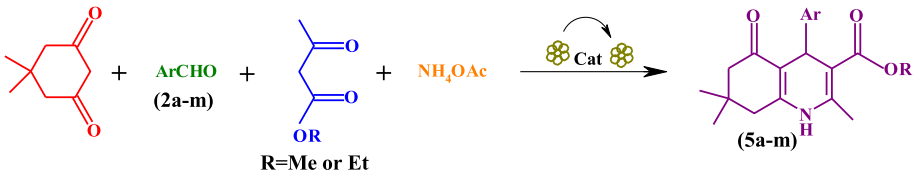

Scheme 1. Synthesis of hexahydroquinolines **5a-m** catalyzed by $Fe_{3-x}Ti_xO_4$-SO_3H MNPs.

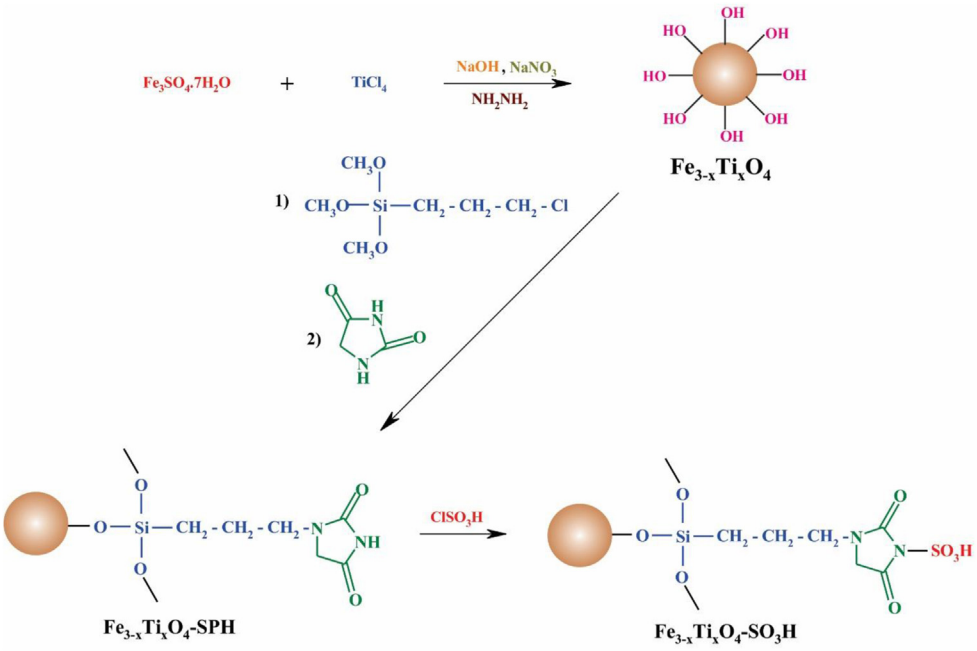

Scheme 2. Synthesis of $Fe_{3-x}Ti_xO_4$-SO_3H MNPs.

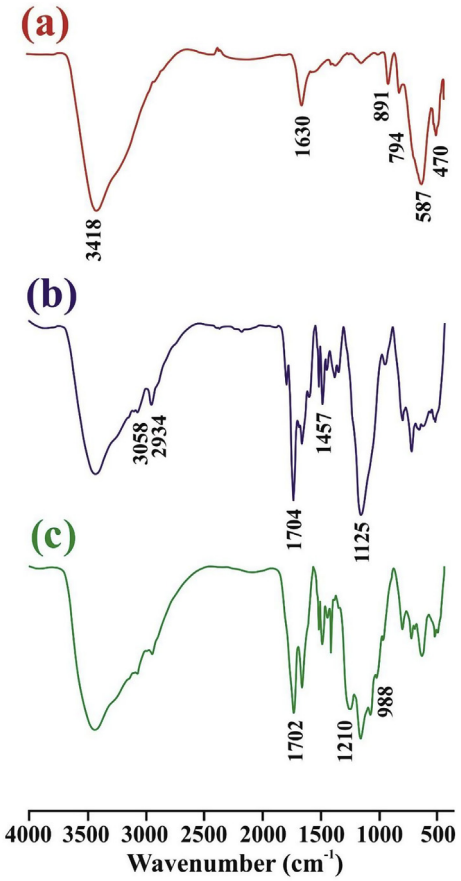

Fig. 1. FTIR spectra of the $Fe_{3-x}Ti_xO_4$ MNPs (a), SPH-functionalized $Fe_{3-x}Ti_xO_4$ (b), and $Fe_{3-x}Ti_xO_4$-SO_3H MNPs (c).

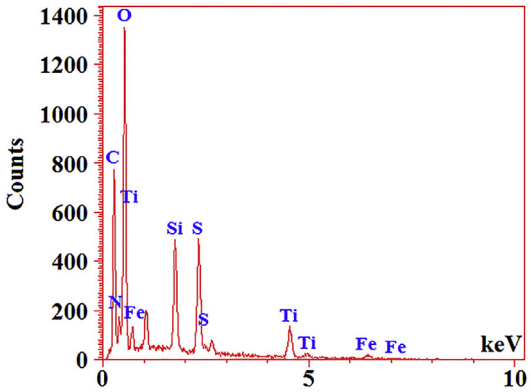

Fig. 2. EDX analysis of $Fe_{3-x}Ti_xO_4$-SO_3H nanocatalyst.

magnetic field (Fig. 5).

The thermal gravimetric (TG) and differential thermal (DT) analyses were performed on the $Fe_{3-x}Ti_xO_4$-SO_3H nanocatalyst to examine its thermal stability (Fig. 6). As evidenced from TGA and DTA curves, the weight loss process of the nanocatalyst is divided into three main stages. The first stage involves the weight loss at 89 °C due to the loss of adsorbed water or any organic solvents that used during the synthesis of the nanocatalyst. A significant weight loss exhibited in the second stage at around 300 °C could be due to the loss of the immobilized sulfamic acid groups. The third weight loss at 415 °C is attributed to complete decomposition of organic residue on the surface of the nanocatalyst. According to thermal property study results, the fabricated nanocatalyst has excellent thermal stability even to apply for various reactions at high temperatures (up to 300 °C).

2.2. Catalytic activity

The fabricated $Fe_{3-x}Ti_xO_4$-SO_3H MNPs were explored as magnetically separable acidic nanocatalyst for the synthesis of

Table 1
Results obtained from EDX analysis.

Sample	C (wt%)	N (wt%)	Si (wt%)	O (wt%)	Fe (wt%)	Ti (wt%)	S (wt%)
$Fe_{3-x}Ti_xO_4$-SO_3H	28.76	13.73	2.81	47.78	0.60	2.46	3.87

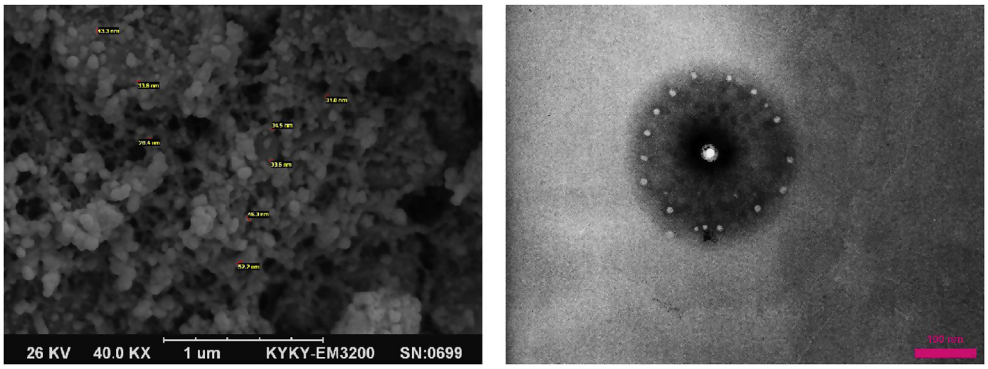

Fig. 3. SEM (left) and TEM (right) images of the synthesized $Fe_{3-x}Ti_xO_4$-SO_3H nanocatalyst.

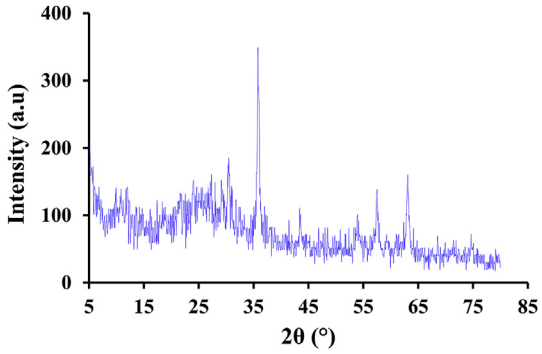

Fig. 4. XRD pattern of the synthesized $Fe_{3-x}Ti_xO_4$-SO_3H nanocatalyst.

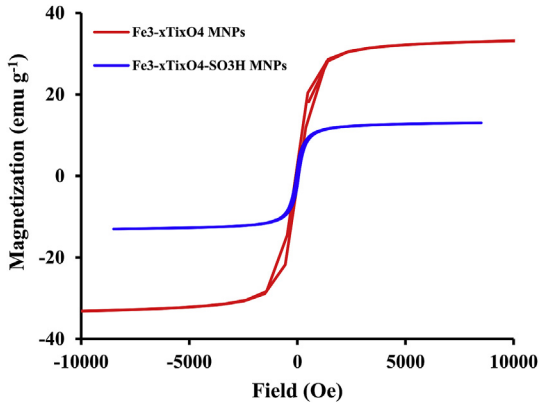

Fig. 5. VSM curves of $Fe_{3-x}Ti_xO_4$ MNPs and $Fe_{3-x}Ti_xO_4$-SO_3H MNPs.

hexahydroquinolines (**5a-m**) from one-pot four-component reaction between aromatic aldehydes, dimedone (5,5-dimethylcyclohexane-1,3-dione), alkyl acetoacetates and ammonium acetate as illustrated in Scheme 1. In order to optimize the reaction conditions, the reaction of dimedone 1, 4-chlorobenzaldehyde (2**b**), ethyl acetoacetate (**3**) and ammonium acetate (**4**) was selected as model reaction. The effects of different reaction parameters were examined as listed in Table 2. The effect of solvent on the reaction was evaluated using some solvents including, H_2O, EtOH and $CHCl_3$ under the same amount (0.01 g) of nanocatalyst loading and noticed that solvent-free condition provided the best result (entry 4). As seen in Table 2, the optimal catalyst loading and reaction temperature in terms of the reaction time (20 min) and yield (94%) were found to be 0.02 g and 60 °C respectively (entry 5). No improvements of the reaction time and yield were observed by further increasing the amount of the nanocatalyst (entries 6 and 7) or reaction temperature (entries 9 and 10). To verify the catalytic importance, the reaction was carried out under the optimized conditions in the absence of the catalyst and it was found that the product was formed in a very low yield (entry 11).

This achievement encouraged us to extend the scope of the described methodology to a series of variously substituted aromatic aldehydes (**2a-m**) in reaction with dimedone **1**, ethyl or methyl acetoacetate **3** and ammonium acetate **4** under the optimized conditions (Table 3). As summarized in Table 3, all the reactions proceeded smoothly to furnish the respective products in relatively short reaction times with excellent and comparable yields irrespective of the nature of the substituent groups bonded to the aromatic ring. All the obtained products (**5a-m**) were known compounds, which were characterized on the basis of their physical and spectral (FTIR, ^{1}H NMR and ^{13}C NMR) analysis and compared with the corresponding data reported in the literature.

2.3. Reaction mechanism

According to the mechanisms proposed in the literature [36,46,65], a plausible reaction pathway to explain the formation of hexahydroquinolines (**5a-m**) is depicted in Scheme 3. First, the $Fe_{3-x}Ti_xO_4$-SO_3H-activated dimedone **1** in its enolized form undergoes nucleophilic condensation with catalyst-activated aldehyde **2** to form the Knoevenagel type intermediate **I**. On the other hand, the alkyl acetoacetate **3** undergoes nucleophilic condensation reaction with ammonium acetate **4** in the presence of the catalyst to produce the enamine intermediate **II**. Then, the nucleophilic addition of the enamine **II** to the catalyst-activated intermediate **I** occurs to provide the intermediate **III**, which undergoes intramolecular nucleophilic cyclization followed by dehydration to furnish the expected products **5**.

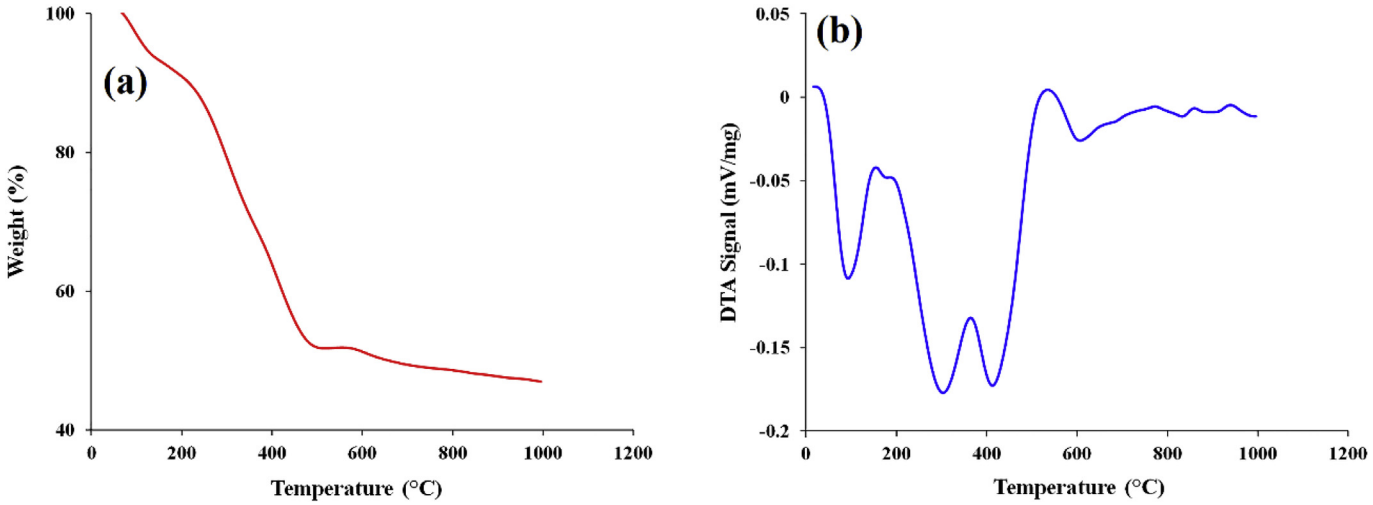

Fig. 6. TGA (a) and DTA (b) curves of the synthesized $Fe_{3-x}Ti_xO_4$-SO_3H nanocatalyst.

Table 2
Screening the reaction parameters for the model reaction of dimedone, 4-chlorobenzaldehyde, ethyl acetoacetate and ammonium acetate[a].

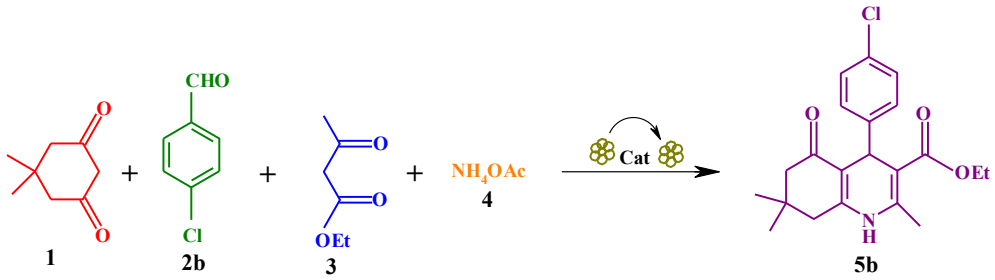

Entry	Catalyst (g)	Solvent	Temperature (°C)	Time (min)	Yield (%)[b]
1	0.01	H_2O	60	60	45
2	0.01	EtOH	60	60	61
3	0.01	$CHCl_3$	60	60	40
4	0.01	–	60	20	85
5	0.02	–	60	20	94
6	0.03	–	60	20	89
7	0.04	–	60	20	87
8	0.02	–	RT	60	56
9	0.02	–	90	20	86
10	0.02	–	110	20	82
11	–	–	60	60	15

[a] Reaction conditions: 4-chlorobenzaldehyde (1 mmol), dimedone (1 mmol), ethyl acetoacetate (1 mmol), ammonium acetate (1.5 mmol), solvent (5 mL).
[b] Isolated pure yield.

2.4. Recyclability of nanocatalyst

The potential recovery and reusability of the nanocatalyst was investigated for the model reaction. The nanocatalyst was recovered simply using an external magnet, washed with ethyl acetate (5 mL) and hot ethanol (10 mL), dried in vacuum at room temperature and reused in the next four subsequent runs. The summarized data in Table 4, demonstrated practical recyclability of the synthesized nanocatalyst with a slight loss of its activity up to four fresh runs.

2.5. Catalyst efficiency

The efficiency of the synthesized $Fe_{3-x}Ti_xO_4$-SO_3H nanocatalyst in comparison with some other catalysts for the synthesis of similar hexahydroquinolines are summarized in Table 5. As seen, in the case of some products the developed $Fe_{3-x}Ti_xO_4$-SO_3H nanocatalyst has higher catalytic performance than those of the reported in the literatures.

3. Experimental

3.1. General

Melting points were measured in open capillary tubes using a BUCHI 510 apparatus. Fourier transform infrared (FTIR) spectra were recorded from KBr pellets using a Shimadzu 435-U-04 FTIR spectrophotometer. ^{1}H NMR and ^{13}C NMR spectra were recorded at

Table 3
$Fe_{3-x}Ti_xO_4$-SO_3H-catalyzed synthesis of hexahydroquinolines **5a-m** under solvent-free condition at 60 °C [a].

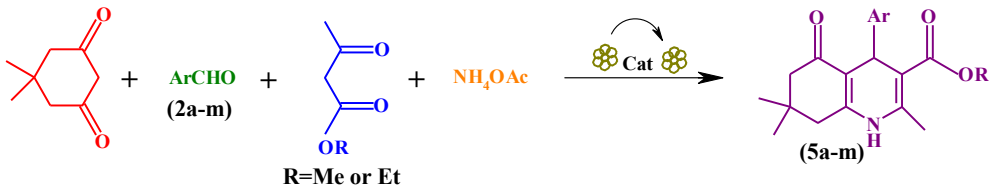

Entry	Ar	Product	R	Time (min)	Yield (%)[b]	Mp (°C)	
						Found	Reported
1	C_6H_5	**5a**	Et	25	85	225–227	–
2	4-ClC_6H_4	**5b**	Et	20	94	245–247	245-246 [62]
3	2-ClC_6H_4	**5c**	Et	25	90	207–209	208-209 [36]
4	3-ClC_6H_4	**5d**	Et	25	91	204–206	209-211 [63]
5	4-FC_6H_4	**5e**	Et	20	93	196–299	184-186 [49]
6	4-$NO_2C_6H_4$	**5f**	Et	25	89	246–248	247-249 [64]
7	4-MeC_6H_4	**5g**	Et	25	98	264–267	262-264 [49]
8	4-$MeOC_6H_4$	**5h**	Et	15	96	256–258	256-258 [46]
9	C_6H_5	**5i**	Me	20	88	263–266	261-263 [65]
10	4-FC_6H_4	**5j**	Me	15	90	245–248	–
11	4-MeC_6H_4	**5k**	Me	10	94	274–277	>270 [66]
12	2-$MeOC_6H_3$	**5l**	Me	10	93	267–270	–
13	2-ClC_6H_4	**5m**	Me	15	92	271–274	271-273 [63]

[a] Conditions: aldehyde (1 mmol), dimedone (1 mmol), ethyl (or methyl) acetoacetate (1 mmol), ammonium acetate (1.5 mmol), catalyst (0.02 g), solvent-free, 60 °C.
[b] Isolated pure yield.

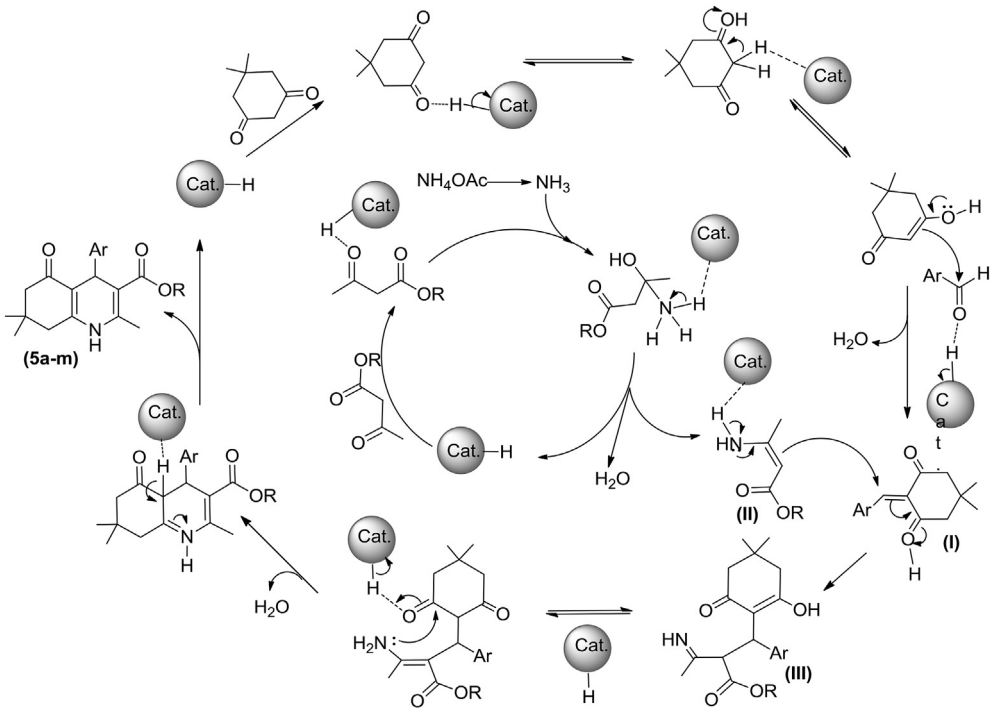

Scheme 3. Proposed mechanism for $Fe_{3-x}Ti_xO_4$-SO_3H-catalyzed synthesis of the hexahydroquinolines (**5a-m**).

250 and 90 MHz, respectively on BRUKER AVANCE instruments using $CDCl_3$ or DSMO-d_6 as solvents at ambient temperature. Scanning electron microscopy (SEM) image was obtained on a KYKY-EM3200 instrument operated at 26 kV accelerating voltage. Transmission electron microscopy (TEM) image was captured on a CM10-TH microscope (Philips, Eindhoven, The Netherlands) with a 100 kV accelerating voltage. Energy-dispersive X-ray (EDX) analysis of the synthesized nanocatalyst was performed on a FE-SEM TESCAN MIRA3-FEG instrument. Thermal properties of the nanocatalyst was investigated in air using TGA/DTA Linseis-181a1750. Magnetic properties of the samples were measured with a vibrating sample magnetometer (VSM, MDKFT, Iran) at room temperature. Ultrasonication was performed in a 2200 ETH-SONICA ultrasound cleaner at a frequency of 45 MHz.

Table 4
Recyclability of the $Fe_{3-x}Ti_xO_4$-SO_3H nanocatalyst for the model reaction between 4-chlorobenzaldehyde, dimedone, ethyl acetoacetate and ammonium acetate.

Run	Time (min)	Yield (%)[a]
1	20	94
2	20	92
3	23	90
4	25	87

[a] Isolated yield.

3.2. Synthesis of $Fe_{3-x}Ti_xO_4$ MNPs

The $Fe_{3-x}Ti_xO_4$ MNPs were synthesized according to our previously reported procedure [53]. In a round-bottomed glass reactor equipped with a reflux condenser, $FeSO_4 \cdot 7H_2O$ (1.90 g, 6.8 mmol) was dissolved in deionized water (10 mL). Afterward, the pH of the solution was reduced to <1 using an HCl solution (1 $molL^{-1}$), then $TiCl_4$ (0.75 mL, 6.8 mmol) and hydrazine monohydrate (2 mL, 41.2 mmol) were added, respectively. The resulted mixture was refluxed at 90 °C under nitrogen atmosphere for about 30 min followed by consecutive dropwise addition a solutions of NaOH (1.60 g) and $NaNO_3$ (0.77 g) in deionized water (10 mL) under vigorous stirring at a rate of 500 rpm for 1 h. Afterward, the resulted mixture was cooled to room temperature, the precipitated $Fe_{3-x}Ti_xO_4$ MNPs were collected using a magnet bar, washed with deionized water several times, and dried in reduced pressure at room temperature.

3.3. Synthesis of the (3-silylpropyl)hydantoin-functionalized $Fe_{3-x}Ti_xO_4$ ($Fe_{3-x}Ti_xO_4$-SPH)

The $Fe_{3-x}Ti_xO_4$-SPH MNPs was synthesized as follows. The $Fe_{3-x}Ti_xO_4$ MNPs (1.00 g) were dispersed in dried pyridine (30 mL) using sonication for 30 min. To the resulted mixture were added a small amount of sodium metal, (3-chloropropyl)-trimethoxysilane (CPTS; 2 mL 10 mmol), and imidazolidine-2,4-dione (hydantoin) (1.50 g, 15 mmol), respectively followed by refluxing under nitrogen atmosphere for about 24 h. Eventually, the reaction mixture was cooled to room temperature to precipitate out the MNPs which were magnetically separated, washed several times with ethanol and dried in vacuum at room temperature.

3.4. Synthesis of $Fe_{3-x}Ti_xO_4$-SO_3H nanocatalyst

The $Fe_{3-x}Ti_xO_4$-SO_3H nanocatalyst was synthesized through the solfunation of $Fe_{3-x}Ti_xO_4$-SPH MNPs. For this purpose, $Fe_{3-x}Ti_xO_4$-SPH MNPs (1.00 g) were dispersed in dried CH_2Cl_2 (15 mL) through the sonication for about 30 min followed by dropwise addition of chlorosulfonic acid (1.5 mL, 22.5 mmol). The resulted reaction mixture was refluxed at room temperature for about 4 h. At the end of this time, the NPs were magnetically separated from the reaction mixture, washed consecutively with CH_2Cl_2 (2 × 5 mL) and ethanol (3 × 5 mL), and dried in reduced pressure at room temperature.

3.5. General procedure for the synthesis of hexahydroquinoline derivatives

A mixture of dimedone **1** (0.140 g, 1 mmol), aldehyde **2** (1 mmol), ethyl or methyl acetoacetate **3** (1 mmol), ammonium acetate **4** (0.115 g, 1.5 mmol), and $Fe_{3-x}Ti_xO_4$-SO_3H nanocatalyst (0.02 g) was stirred at 60 °C under solvent-free condition for the appropriate time (Table 3). After completion of the reaction (monitored by TLC), the reaction mixture was diluted with hot ethanol (10 mL) and stirred until the solid materials dissolved completely. The nanocatalyst was recovered magnetically using a magnetic bar. The remaining supernatant was diluted with water (20 mL) and cooled to room temperature to precipitate the products **5a-m**, which were filtered and purified by recrystallization from a hot mixed ethanol/water (3:2 v/v) to afford the pure products. All the products synthesized are known compounds, which were characterized by their melting points and spectral (FTIR, and $^1H/^{13}C$ NMR) analyses and compared with their corresponding data reported in the literature.

Table 5
The efficiency of the $Fe_{3-x}Ti_xO_4$-SO_3H nanocatalyst in comparison with some other catalyst that employed to the synthesis of hexahydroquinoline derivatives.

Sample	Catalyst	Condition	Temperature (°C)	Time (min)	Yield (%)	References
5a	$Fe_{3-x}Ti_xO_4$-SO_3H	Solvent-free	60	25	85	**Current**
5a	*t*-BuOK	Solvent-free	60	120	73	[67]
5a	$K_7[PW_{11}CoO_{40}]$	CH_3CN	reflux	35	80	[68]
5b	$Fe_{3-x}Ti_xO_4$-SO_3H	Solvent-free	60	20	94	**Current**
5b	$K_7[PW_{11}CoO_{40}]$	CH_3CN	reflux	30	85	[68]
5b	*p*-TSA	EtOH	r.t.	120	90	[69]
5b	SSA	Solvent-free	60 or MW	30	91	[70]
5b	ANP	EtOH	r.t.	240	88	[71]
5f	$Fe_{3-x}Ti_xO_4$-SO_3H	Solvent-free	60	25	89	**Current**
5f	Nano MgO	EtOH	reflux	100	75	[72]
5f	$K_7[PW_{11}CoO_{40}]$	CH_3CN	reflux	30	80	[68]
5g	$Fe_{3-x}Ti_xO_4$-SO_3H	Solvent-free	60	25	98	**Current**
5g	SBA-Pr-SO_3H	Solvent-free	80	10	90	[73]
5g	SO_3H-KIT-5	Solvent-free	90	70	89	[74]
5g	SBISAC	Solvent-free	50	9	90	[46]
5g	nano-Fe_3O_4	Solvent-free	50	7	89	[35]
5g	PPA-SiO_2	Solvent-free	80	60	90	[75]
5g	ANP	EtOH	r.t.	240	82	[71]
5g	DBH or DCH	Solvent-free	130	30(35)	86(82)	[76]
5g	$SnCl_2 \cdot 2H_2O$	Solvent-free	80	5	86	[77]
5g	*t*-BuOK	Solvent-free	60	120	92	[67]
5g	$Sc(OTf)_3$	EtOH	r.t.	360	87	[48]
5h	$Fe_{3-x}Ti_xO_4$-SO_3H	Solvent-free	60	15	96	**Current**
5h	CuO NPs	Solvent-free	140	38	85	[78]
5h	*t*-BuOK	Solvent-free	60	60	85	[67]

SBA-Pr-SO_3H: sulfonic acid functionalized SBA-15; ANP: hreo-(1S,2S)-2-amino-1-(40-nitrophenyl)-1,3-propanediol; *p*-TSA: *p*-toluenesulfonic acid; SSA: silica sulfuric acid; SBISAC: silica-bonded imidazolium-sulfonic acid chloride.

3.5.1. Selected physical and spectral data

*3.5.1.1. Ethyl 2,7,7-trimethyl-4-(4-nitrophenyl)-5-oxo-1,4,5,6,7,8-hexahydroquinoline-3- carboxylate (**5f**).* Yellow solid (342 mg, 89%); m.p. 246–248 °C; FTIR (KBr) ν: 3276, 3187, 3072, 2966, 1703, 1651, 1607, 1493, 1344, 1215, 1068, 830, 532 cm^{-1}; ^1H NMR (250 MHz, $CDCl_3$) δ: 0.89 (s, 3H, CH_3), 1.06 (s, 3H, CH_3), 1.14–1.19 (t, 3H, CH_3), 2.08–2.40 (m, 7H, $2CH_2$, CH_3), 3.99–4.08 (q, 2H, CH_2), 5.14 (s, 1H, CH), 6.65 (s, 1H, NH), 7.46–7.49 (d, 2H, Ar–H), 8.05–8.08 (d, 2H, Ar–H) ppm; ^{13}C NMR (62.90 MHz, $CDCl_3$) δ: 14.1, 19.3, 27.0, 29.3, 32.6, 37.2, 40.8, 50.6, 60.0, 104.8, 110.9, 123.3, 128.9, 144.6, 146.1, 149.1, 154.5, 166.8, 195.5 ppm.

*3.5.1.2. Ethyl 4-(4-methoxyphenyl)-2,7,7-trimethyl-5-oxo-1,4,5,6,7,8-hexahydroquinoline-3- carboxylate (**5h**).* Pale yellow solid (355 mg, 96%); m.p. 256–258 °C; FTIR (KBr) ν: 3276, 3204, 3078, 2957, 1701, 1651, 1605, 1496, 1380, 1280, 1215, 1032, 850, 537 cm^{-1}; ^1H NMR (250 MHz, $CDCl_3$) δ: 0.91 (s, 3H, CH_3), 1.03 (s, 3H, CH_3), 1.18–1.23 (t, 3H, CH_3), 2.08–2.31 (m, 7H, $2CH_2$, CH_3), 3.70 (s, 3H, CH_3), 4.02–4.10 (q, 2H, CH_2), 4.98 (s, 1H, CH), 6.70–6.73 (d, 2H, H–Ar), 7.04 (s, 1H, NH), 7.19–7.22 (d, 2H, Ar–H) ppm; ^{13}C NMR (62.90 MHz, $CDCl_3$) δ: 14.2, 19.1, 27.0, 29.4, 32.6, 35.7, 40.6, 50.7, 55.0, 59.7, 106.12, 111.9, 113.2, 128.9, 139.7, 143.6, 149.0, 157.7, 167.6, 195.9 ppm.

*3.5.1.3. Methyl 4-(4-fluorophenyl)-2,7,7-trimethyl-5-oxo-1,4,5,6,7,8-hexahydroquinoline-3- carboxylate (**5j**).* Pale yellow solid (310 mg, 90%); m.p. 245–248 °C; FTIR (KBr) ν: 3262, 3196, 3072, 2962, 1709, 1679, 1644, 1609, 1501, 1383, 1227, 1169, 1115, 1005, 847, 769, 650, 612, 542 cm^{-1}; ^1H NMR (250 MHz, DMSO-d_6) δ: 0.80 (s, 3H, CH_3), 0.98 (s, 3H, CH_3), 1.93–2.47 (m, 7H, $2CH_2$, CH_3), 3.50 (s, 3H, CH_3), 4.85 (s, 1H, CH), 6.94–6.97 (d, 2H, Ar–H), 7.12–7.14 (d, 2H, Ar–H), 9.09 (s, 1H, NH) ppm; ^{13}C NMR (62.90 MHz, DMSO-d_6) 18.7, 26.8, 29.5, 32.5, 35.5, 50.6, 51.1, 103.5, 110.4, 114.7, 115.0, 129.3, 129.4, 144.1, 144.15, 145.9, 149.9, 158.9, 162.8, 167.6, 194.7 ppm.

*3.5.1.4. Methyl 4-(2-methoxyphenyl)-2,7,7-trimethyl-5-oxo-1,4,5,6,7,8-hexahydroquinoline- 3-carboxylate (**5l**).* White solid (331 mg, 93%); m.p. 267–270 °C; FTIR (KBr) ν: 3283, 3213, 3076, 2957, 1692, 1640, 1622, 1609, 1485, 1378, 1218, 1171, 1028, 761, 515 cm^{-1}; ^1H NMR (250 MHz, DMSO-d_6) δ: 0.82 (s, 3H, CH_3), 0.97 (s, 3H, CH_3), 1.84–2.47 (m, 7H, $2CH_2$, CH_3), 3.45 (s, 3H, CH_3), 3.67 (s, 3H, CH_3), 5.02 (s, 1H, CH), 6.73–7.02 (m, 4H, Ar–H), 8.96 (s, 1H, NH) ppm; ^{13}C NMR (62.90 MHz, DMSO-d_6) 18.4, 26.6, 29.7, 32.4, 32.9, 50.8, 55.7, 103.4, 109.0, 111.5, 120.1, 127.4, 130.5, 135.4, 144.4, 150.5, 157.4, 168.2, 194.2 ppm.

4. Conclusions

In summary, we have successfully synthesized $Fe_{3-x}Ti_xO_4$-SO_3H MNPs as magnetic acidic nanocatalyst from a simple three-step procedure and fully characterized by FTIR spectroscopy, EDX, SEM, TEM, XRD, TGA, and VSM analyses. The fabricated MNPs conveniently catalyzed the one-pot four-component reaction of aromatic aldehydes, dimedone, ethyl or methyl acetoacetate and ammonium acetate for the synthesis of hexahydroquinoline derivatives in excellent yields with preserving atom economy. The prominent advantages of this new protocol are the ease of separation and recyclability of the nanocatalyst (up to four new subsequent runs), operational simplicity, high yields of the products, short reaction time, and environmental benignity avoiding toxic reagents and volatile solvents.

Note

The authors declare no competing financial interest.

Acknowledgment

The authors wish to thank the Research Council of the Bu-Ali Sina University (Hamedan, Iran) for instrumental and technical supports to carry out this research.

Appendix A. Supplementary data

Supplementary data to this article can be found online at https://doi.org/10.1016/j.jorganchem.2019.05.020.

References

[1] H. Duan, D. Li, Y. Wang, Chem. Soc. Rev. 44 (2015) 5778–5792.
[2] P.T. Anastas, T. Williamson, Green Chemistry: Frontiers in Benign Chemical Synthesis and Process, Oxford University Press, Oxford, U. K, 1998.
[3] X. Wu, C. Lu, Z. Zhou, G. Yuan, R. Xiong, X. Zhang, Environ. Sci. Nano. 1 (2014) 71–79.
[4] N. Poorgholy, B. Massoumi, M. Ghorbani, M. Jaymand, H. Hamishehkar, Drug Dev. Ind. Pharm. 8 (2018) 1254–1261.
[5] (a) M. Mohssenimehr, M. Mamaghani, F. Shirini, M. Sheykhan, Chin. Chem. Lett. 25 (2014) 1387–1391;
(b) S. Shylesh, V. Schunemann, W.R. Thiel, Angew. Chem. Int. Ed. 49 (2010) 3428–3459.
[6] L.M. Rossi, N.J.S. Costa, F.P. Silva, R.V. Goncalves, Nanotechnol. Rev. 2 (2013) 597–614.
[7] R.B. Nasir-Baig, R.S. Varma, Chem. Commun. 49 (2013) 752–770.
[8] Q. Dong, Z. Meng, C.L. Ho, H. Guo, W. Yang, I. Manners, L. Xu, W.Y. Wong, Chem. Soc. Rev. 47 (2018) 4934–4953.
[9] R. Mohammadi, S. Esmati, M. Gholamhosseini-Nazari, R. Teimuri-Mofrad, New J. Chem. 43 (2019) 135–145.
[10] M. Ma, Y. Yang, D. Liao, P. Lyu, J. Zhang, J. Liang, L. Zhang, Appl. Organomet. Chem. 33 (2019), e4708.
[11] L. Ma'mani, M. Sheykhan, A. Heydari, M. Faraji, Y. Yamini, Appl. Catal., A 377 (2010) 64–69.
[12] Z. Meng, G. Li, N. Zhu, C.L. Ho, C.W. Leung, W.Y. Wong, J. Organomet. Chem. 849–850 (2017) 10–16.
[13] F. Shi, M.K. Tse, M.M. Pohl, A. Bruckner, S. Zhanga, M. Beller, Angew. Chem. Int. Ed. 46 (2007) 8866–8868.
[14] D.H. Zhang, G.D. Li, J.X. Li, J.S. Chen, Chem. Commun. 29 (2008) 3414–3416.
[15] K. Liu, C.L. Ho, S. Aouba, Y.Q. Zhao, Z.H. Lu, S. Petrov, N. Coombs, P. Dube, H.E. Ruda, W.Y. Wong, I. Manners, Angew. Chem. Int. Ed. 47 (2008) 1255–1259.
[16] A. Saxena, A. Kumar, S. Mozumdar, J. Mol. Catal. A. 269 (2007) 35–40.
[17] N. Zhu, H. Ji, P. Yu, J. Niu, M.U. Farooq, M.W. Akram, I.O. Udego, H. Li, X. Niu, Nanomaterials 8 (2018) 810.
[18] C. Yuan, Z. Huang, J. Chen, J. Catal. Commun. 24 (2012) 56–60.
[19] D. Guin, B. Baruwati, S.V. Manorama, Org. Lett. 9 (2007) 1419–1421.
[20] J.A. Gladysz, Chem. Rev. 102 (2002) 3215–3216.
[21] Z. Mozafari, B. Massoumi, M. Jaymand, J. Appl. Polym. Sci. 135 (2018) 46657.
[22] M. Hatamzadeh, M. Johari-Ahar, M. Jaymand, Int. J. Nanosci. Nanotechnol. 8 (2012) 51–60.
[23] D. Azarifar, R. Asadpoor, O. Badalkhani, M. Jaymand, E. Tavakoli, M. Bazouleh, ChemistrySelect 3 (2018) 13722–13728.
[24] N. Li, Z. Ji, L. Chen, X. Shen, Y. Zhang, S. Cheng, H. Zhou, Appl. Surf. Sci. 462 (2018) 1–7.
[25] A. Naikwade, M. Jagadale, D. Kale, S. Gajare, G. Rashinkar, Catal. Lett. 148 (2018) 3178–3192.
[26] D. Azarifar, O. Badalkhani, Y. Abbasi, J. Sulfur Chem. 37 (2016) 656–673.
[27] S. Campelj, D. Makovec, M. Drofenik, J. Magn. Magn. Mater. 321 (2009) 1346–1350.
[28] S. Kralj, M. Drofenik, D. Makovec, J. Nanoparticle Res. 13 (2011) 2829–2841.
[29] N. Koukabi, E. Kolvari, M.A. Zolfigol, A. Khazaei, B. Shirmardi-Shaghasemi, B. Fasahati, Adv. Synth. Catal. 354 (2012) 2001–2008.
[30] C.T. Yavuz, J.T. Mayo, W.W. Yu, A. Prakash, J.C. Falkner, S. Yean, L.L. Cong, H.J. Shipley, A. Kan, M. Tomson, D. Natelson, V.L. Colvin, Science 314 (2006) 964–967.
[31] A. Hu, G.T. Yee, W. Lin, J. Am. Chem. Soc. 127 (2005) 12486–12487.
[32] A.K. Tucker-Schwartz, R.L. Garrell, Chem. Eur J. 16 (2010) 12718–12726.
[33] S. Luo, X. Zheng, H. Xu, X. Mi, L. Zhang, J.P. Cheng, Adv. Synth. Catal. 349 (2007) 2431–2434.
[34] V. Polshettiwar, R. Luque, A. Fihri, H. Zhu, M. Bouhrara, J.M. Basset, Chem. Rev. 111 (2011) 3036–3075.
[35] A. Khazaei, A.R. Moosavi-Zare, H. Afshar-Hezarkhani, V. Khakyzadeh, RSC Adv. 4 (2014) 32142–32147.
[36] (a) D. De, F.M. Krogstad, L.D. Byers, D.J. Krogstad, J. Med. Chem. 41 (1998) 4918–4926;
(b) P.A. Stocks, K.J. Raynes, P.G. Bray, B.K. Park, P.M. O'Neill, S.A. Ward, J. Med. Chem. 45 (2002) 4975–4983;
(c) J.L. Vennerstrom, A.L. Ager Jr., A. Dorn, S.L. Andersen, L. Gerena, R.G. Ridley, W.K. Milhous, J. Med. Chem. 41 (1998) 4360–4364;

(d) C.H. Kaschula, T.J. Egan, R. Hunter, N. Basilico, S. Parapini, D. Taramelli, E. Pasini, D. Monti, J. Med. Chem. 45 (2002) 3531–3539;
(e) S. Delarue, S. Girault, L. Maes, M.A. Debreu-Fontaine, M. Labaeid, P. Grellier, C. Sergheraert, J. Med. Chem. 44 (2001) 2827–2833.
[37] S. Pomel, F. Dubar, D. Forge, P.M. Loiseau, C. Biot, Bioorg. Med. Chem. 23 (2015) 5168–5174.
[38] K.L. Kees, J.J. Fitzgerald, K.E. Steiner, J.F. Mattes, B. Mihan, T. Tosi, D. Mondoro, M.L. McCaleb, J. Med. Chem. 39 (1996) 3920–3928.
[39] B. Cottineau, P. Toto, C. Marot, A. Pipaud, J. Chenault, Bioorg. Med. Chem. Lett 12 (2002) 2105–2108.
[40] J.N. Kim, Y.M. Chung, Y.J. Im, Tetrahedron 57 (2001) 2507–2514.
[41] A.K. Agrawal, S.A. Jenekhe, L. Lu, M.M. Alam, Macromolecules 34 (2001) 7315–7324.
[42] (a) G. Jones, in: A.R. Katritzky, C.W. Rees (Eds.), Comprehensive Hterocyclic Chemistry II vol. 5, Pergamon Press, New York, 1996, p. 167;
(b) B. Jiang, Y.G. Si, J. Org. Chem. 67 (2002) 9449–9451.
[43] P. Friedländer, Tetrahedron Lett. 43 (2002) 3907–3910.
[44] (a) R.P. Thummel, Synlett 1 (1992) 1–12;
(b) S. Gladiali, G. Chelucci, M.S. Mudadu, M.A. Gsataut, R.P. Thummel, J. Org. Chem. 66 (2001) 400–405.
[45] M.A. Zolfigol, P. Salehi, A. Ghaderi, M. Shiri, Catal. Commun. 8 (2007) 1214–1218.
[46] A.R. Moosavi-Zare, M.A. Zolfigol, M. Zarei, A. Afsar, J. Appl. Catal A. 505 (2015) 224–234.
[47] M. Hong, C. Cai, W.B.J. Yi, J. Fluorine Chem. 131 (2010) 111–114.
[48] J.L. Donelson, R.A. Gibbs, S.K. De, J. Mol. Catal. A. 256 (2006) 309–311.
[49] M. Tajbakhsh, H. Alinezhad, M. Norouzi, S. Baghery, M. Akbari, J. Mol. Liq. 177 (2013) 44–48.
[50] M.B. Gawande, V.D.B. Bonifácio, R.S. Varma, I.D. Nogueira, N. Bundaleski, C.A.A. Ghumman, N.D. Teodorod, P.S. Branco, Green Chem. 15 (2013) 1226–1231.
[51] M.A. Zolfigol, H. Ghaderi, S. Baghery, L. Mohammadi, J. Iran. Chem. Soc. 14 (2017) 121–134.
[52] M. Mamaghani, M. Jamali-Moghadam, R. Hosseinnia, J. Iran. Chem. Soc. 14 (2017) 395–401.
[53] D. Azarifar, Y. Abbasi, Synth. Commun. 46 (2016) 745–758.
[54] D. Azarifar, Y. Abbasi, O. Badalkhani, J. Iran. Chem. Soc. 13 (2016) 2029–2038.
[55] A. Azarifar, R. Nejat-Yami, M. AlKobaisi, D. Azarifar, J. Iran. Chem. Soc. 10 (2013) 439–446.
[56] D. Azarifar, R. Nejat-Yami, F. Sameri, Z. Akrami, Lett. Org. Chem. 9 (2012) 435–439.
[57] D. Azarifar, M. Ghaemi, M. Golbaghi, R. Karamian, M. Asadbegy, RSC Adv. 6 (2016) 92028–92039.
[58] D. Azarifar, O. Badalkhani, Y. Abbasi, M. Hasanabadi, J. Iran. Chem. Soc. 14 (2017) 403–418.
[59] X. Liang, Y. Zhong, S. Zhu, L. Ma, P. Yuan, J. Zhu, H. He, Z. Jiang, J. Hazard Mater. 199–200 (2012) 247–254.
[60] M.B. Gawande, A.K. Rathi, I.D. Nogueira, R.S. Varma, P.S. Branco, Green Chem. 15 (2013) 1895–1899.
[61] F. Nemati, M.M. Heravi, R. Saeedi-Rad, Chin. J. Catal. 33 (2012) 1825–1831.
[62] A. Heydari, S. Khaksar, M. Tajbakhsh, H.R. Bijanzadeh, J. Fluorine Chem. 130 (2009) 609–614.
[63] B.X. Du, Y.L. Li, X.S. Wang, M.M. Zhang, D.Q. Shi, S.J. Tu, Chin. J. Org. Chem. 26 (2006) 698–701.
[64] A. Zare, F. Abi, A.R. Moosavi-Zare, M.H. Beyzavi, M.A. Zolfigol, J. Mol. Liq. 178 (2013) 113–121.
[65] A. Khazaei, M.A. Zolfigol, A.R. Moosavi-Zare, J. Afsar, A. Zare, V. Khakyzadeh, M.H. Beyzavi, Chin. J. Catal. 34 (2013) 1936–1944.
[66] A. Kumar, R.A. Maurya, Tetrahedron 63 (2007) 1946–1952.
[67] A. Debache, L. Chouguiat, R. Boulcina, B. Carboni, Open Org. Chem. J. 6 (2012) 12–20.
[68] M.M. Heravi, K. Bakhtiari, N.M. Javadi, F.F. Bamoharram, M. Saeedi, H.A. Oskooie, J. Mol. Catal. A. 264 (2007) 50–52.
[69] S.R. Cherkupally, R. Mekala, Chem. Pharm. Bull. 56 (2008) 1002–1004.
[70] A. Mobinikhaledi, N. Foroughifar, M.A. Bodaghifard, H. Moghanian, S. Ebrahimi, M. Kalho, Synth. Commun. 39 (2009) 1166–1174.
[71] S.J. Song, Z.X. Shan, Y. Jin, Synth. Commun. 40 (2010) 3067–3077.
[72] H. Mirzaee, A. Izadyar, A. Davoodnia, H. Eshghi, J. Appl Chem. Res. 8 (2014) 57–63.
[73] G. Mohammadi-Ziarani, A.R. Badiei, Y. Khaniania, M. Haddadpour, Iran. J. Chem. Chem. Eng. 29 (2010) 1–10.
[74] R. Mirsafaei, S. Delzendeh, A. Abdolazimi, Int. J. Environ. Sci. Technol. 13 (2016) 2219–2226.
[75] A. Khojastehnezhad, F. Moeinpour, A. Davoodnia, Chin. Chem. Lett. 22 (2011) 807–811.
[76] B. Maleki, R. Tayebee, M. Kermanian, S. Sedigh-Ashrafi, J. Mex. Chem. Soc. 57 (2013) 290–297.
[77] N. Surekha, Deshmukh, B. Jitendra, A. Gujar, Mane Ramrao, S. Murlidhar, Shingare, Iran. J. Catal. 6 (2016) 89–94.
[78] J. Safaei-Ghomi, M.A. Ghasemzadeh, J. Nanostruct. 1 (2012) 243–248.